ISSN 1063-7761, Journal of Experimental and Theoretical Physics, 2006, Vol. 102, No. 2, pp. 355–364. © Pleiades Publishing, Inc., 2006
Original Russian Text © S.P. Kuznetsov, E.P. Seleznev, 2006, published in Zhurnal Éksperimental'noĭ i Teoreticheskoĭ Fiziki, 2006, Vol. 129, No. 2, pp. 400–412.

STATISTICAL, NONLINEAR, AND SOFT MATTER PHYSICS

A Strange Attractor of the Smale–Williams Type in the Chaotic Dynamics of a Physical System

S. P. Kuznetsov* and E. P. Seleznev

Saratov Branch, Institute of Radio Engineering and Electronics, Russian Academy of Sciences, Saratov, 410019 Russia

**e-mail: spkuz@rambler.ru*

Received August 11, 2005

Abstract—A nonautonomous nonlinear system is constructed and implemented as an experimental device. As represented by a 4D stroboscopic Poincaré map, the system exhibits a Smale–Williams-type strange attractor. The system consists of two coupled van der Pol oscillators whose frequencies differ by a factor of two. The corresponding Hopf bifurcation parameters slowly vary as periodic functions of time in antiphase with one another; i.e., excitation is alternately transferred between the oscillators. The mechanisms underlying the system's chaotic dynamics and onset of chaos are qualitatively explained. A governing system of differential equations is formulated. The existence of a chaotic attractor is confirmed by numerical results. Hyperbolicity is verified numerically by performing a statistical analysis of the distribution of the angle between the stable and unstable subspaces of manifolds of the chaotic invariant set. Experimental results are in qualitative agreement with numerical predictions.

PACS numbers: 05.45.–a

DOI: 10.1134/S1063776106020166

1. INTRODUCTION

In the mathematical theory of chaotic dynamics based on a rigorous axiomatic approach, hyperbolicity means that all trajectories in the invariant set are of saddle type, with well-defined stable and unstable manifolds [1–7]. Dissipative (phase-volume contracting) hyperbolic systems exhibit strange attractors with strong chaotic properties. The examples of hyperbolic attractors discussed in textbooks and monographs on nonlinear dynamics, such as Plykin's attractor or Smale–Williams' solenoid, are constructed by using artificial mathematical models [1–8].

The Smale–Williams solenoid is generated by a dissipative dynamical system that maps a three-dimensional phase space into itself iteratively as illustrated by Fig. 1. Suppose that the 3D torus shown in Fig. 1a behaves as a plastic doughnut. It is stretched to twice its original length, folded in half, and squeezed into its original volume as in Fig. 1b. This is possible only if the area of its cross section transverse to the stretching direction reduces by more than half. Since the doughnut's volume contracts accordingly, the dynamical system must be dissipative. The cross sections of the sets obtained by repeating this procedure make up a sequence of nested disks whose number doubles at each iteration step as each disk is cropped into two smaller ones that are contained in it. Figures 1c and 1d depict, respectively, the result of two iteration steps and the Smale–Williams solenoid, with a fractal cross section similar to the Cantor set, generated as the process is continued ad infinitum.

It has been proved that hyperbolic strange attractors, such as the Smale–Williams solenoid, are structurally stable [1–5]. Structural stability means robustness of solutions to the governing dynamical equations under changes in control-parameter values. In particular, the Cantor-like structure of the hyperbolic strange attractor is preserved if the changes are sufficiently small. The high sensitivity of chaotic dynamics to initial conditions is quantified by the Lyapunov exponent, which smoothly depends on control parameters and never drops to negative values as it typically does in the case of a nonhyperbolic attractor.

The mathematical theory of hyperbolic chaos does not seem to have been convincingly applied to any physical system, even though its concepts are commonly invoked to explain chaotic behavior of realistic nonlinear systems.

On the other hand, the complex dynamics of physically plausible nonlinear models (autonomous or periodically forced nonlinear oscillators, the Rössler system, and the like) are not completely hyperbolic [7–10]. "Chaotic" behavior of this kind is generally associated with the so-called quasi-attractor, which contains not only chaotic, but also stable periodic orbits with large periods. (Usually, orbits of the latter type cannot be captured numerically because their basins of attraction are narrow [7–10].) While rigorous mathematical description of quasi-attractors remains an open prob-

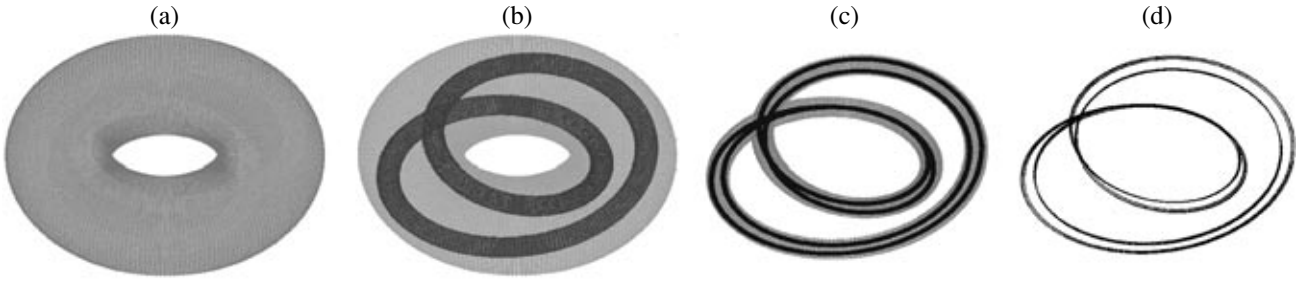

Fig. 1. Generation of an attractor by mapping a 3D phase space into itself: a solid torus (a) is stretched to twice its original length, folded in half, contracted in the transverse direction, and squeezed into its original volume (b); (c) the image of the original torus after two iteration steps; (d) the Smale–Williams solenoid generated by continuing the iterative process ad infinitum.

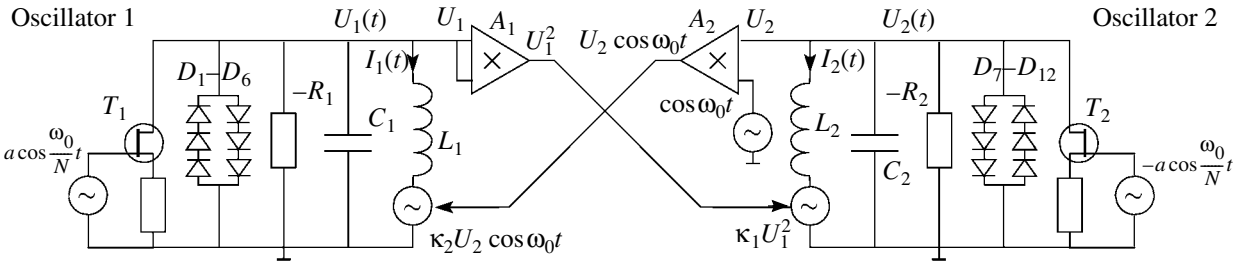

Fig. 2. Circuit diagram of a device consisting of two coupled van der Pol oscillators with periodically varying parameters: a physical system having a Smale–Williams-type strange attractor.

lem, nonhyperbolic dynamics of physical systems are obscured by noise. It has been proved that the chaotic attractor in the Lorenz system corresponding to a certain set of parameter values exhibits the key properties of hyperbolic attractors. However, the system does not fully comply with the axioms underlying the theory of hyperbolic chaos, and the attractor has been classified as a quasi-hyperbolic one [11, 12].

Examples of hyperbolic chaos in dynamical systems described by differential equations have been discussed in just a few theoretical studies. It was found in [13] that the frictionless motion of a mechanical system called *triple linkage* can be described in terms of a geodesic flow on a surface with everywhere negative Gaussian curvature. In the presence of friction, the system, supplemented with an appropriate feedback control, is expected to have a hyperbolic chaotic attractor. In [14], an artificial 3D flow was constructed that has Plykin's attractor as represented by the corresponding Poincaré map. However, that example was too complicated to be implemented in a physical system. In [15], it was argued that the Poincaré map defined by a 3D flow constructed as a neuron model exhibits a Plykin-like attractor.

In this paper, a simple and transparent example of a nonautonomous physical system is constructed for which the existence of a hyperbolic strange attractor follows from the qualitative argumentation and numerical analysis presented here. As represented by a stroboscopic Poincaré map, it is analogous to the Smale–Williams solenoid embedded in a four-dimensional phase space.

2. DESIGN AND OPERATING PRINCIPLE OF A SYSTEM BASED ON COUPLED VAN DER POL OSCILLATORS

The electronic device schematized by the circuit diagram shown in Fig. 2 is a nonautonomous system combining two van der Pol oscillators with free-running frequencies ω_0 and $2\omega_0$. Each oscillator contains a coil of inductance $L_{1,2}$ and a capacitor of capacitance $C_{1,2}$ making up an oscillating circuit, so that

$$\omega_0 = \frac{1}{\sqrt{L_1 C_1}}, \quad 2\omega_0 = \frac{1}{\sqrt{L_2 C_2}}.$$

Negative-resistance components based on operational amplifiers are introduced whose respective resistances, $-R_{1,2}$, can be treated as constant parameters in the entire operating voltage ranges of the corresponding oscillating circuits. A nonlinear conductance that ensures increase in energy loss with oscillation amplitude is implemented in a circuit component consisting of two oppositely poled parallel arrays of series-connected semiconductor diodes. A field-effect transistor is used as an almost linearly conducting component, with drain current controlled by the gate voltage slowly

varying as a periodic function of time with period $T = 2\pi N/\omega_0$, where N is an integer. During successive half-periods of its variation, one oscillator is active while the other is idle and vice versa. Voltage squarer A_1 in oscillator *1* generates a second harmonic signal, which triggers the active oscillator *2* into oscillation in a frequency range around $2\omega_0$. Detector A_2 heterodynes the output of oscillator *2* with an auxiliary signal of frequency ω_0 to produce a difference-frequency signal resonant with the frequency of oscillator *1*, which triggers oscillator *1* when it becomes active. Thus, excitation is alternately transferred between the oscillators.

The circuit functions as a chaos generator as follows. Suppose that the signal generated by the active oscillator *1* has a phase φ: $U_1 \propto \cos(\omega_0 t + \varphi)$. Then, the output U_1^2 of voltage squarer A_1 contains the second harmonic $\cos(2\omega_0 t + 2\varphi)$ with phase 2φ. When oscillator *2* becomes active, the generated signal U_2 has the phase 2φ. After this signal is heterodyned with the auxiliary signal by means of detector A_2, the resulting single-frequency signal has the same phase 2φ. Thus, the signal generated by oscillator *1* during the next half-period of its operation has the phase 2φ. It is obvious that the phases of the signals generated by oscillator *1* during subsequent half-periods can be represented, at least approximately, by the sawtooth map

$$\varphi_{n+1} = 2\varphi_n, \quad \mod(2\pi), \tag{1}$$

which exhibits chaotic dynamics [1, 4, 6, 7]. In particular, Eq. (1) obviously implies that a small deviation from the initial state doubles at each iteration step. This sensitivity to initial conditions is a key indicator of chaotic dynamics.

The dynamics of the coupled oscillators can be studied by analyzing the sequence of instantaneous states generated by a stroboscopic map of the 4D phase space into itself with the period T. Indeed, the state of the system at any instant can be described by four variables (the voltages and currents in both oscillating circuits): $\mathbf{V} = \{U_1, I_1, U_2, I_2\}$. Therefore, if the vector $\mathbf{V} = \mathbf{V}_n$ is given at $t = nT$, then the dynamical system uniquely determines the state variables at the next point of stroboscopic section: $\mathbf{V}_{n+1} = \mathbf{F}(\mathbf{V}_n)$.

In the 4D state space, the eigendirection associated with the phase φ is expanding and the remaining three are contracting. As a geometrical illustration, consider a 4D solid toroid (direct product of a 1D circle with a 3D ball). At each step of the stroboscopic map $\mathbf{V}_{n+1} = \mathbf{F}(\mathbf{V}_n)$, it is stretched to twice its original length, contracted in the transverse direction, folded in half, and squeezed into its original volume. The complete analogy of this process to the construction of the Smale–Williams solenoid suggests that the system under analysis has a hyperbolic chaotic attractor. The numerical results presented below corroborate this conjecture.

3. GOVERNING SYSTEM OF DIFFERENTIAL EQUATIONS

To derive the system of equations describing the dynamics of the circuit, we write Kirchhoff's current-balance law and the equation relating the current through the coil to the voltage across it for each subsystem:

$$\begin{aligned}
&C_1\frac{dU_1}{dt} + I_1 - \frac{U_1}{R_1} + f(U_1) \\
&+ U_1\left(g_1 - k_1 a\cos\frac{\omega_0 t}{N}\right) = 0, \\
&L_1\frac{dI_1}{dt} = U_1 + \kappa_2 U_2\cos\omega_0 t, \\
&C_2\frac{dU_2}{dt} + I_2 - \frac{U_2}{R_2} + f(U_2) \\
&+ U_2\left(g_2 + k_2 a\cos\frac{\omega_0 t}{N}\right) = 0, \\
&L_2\frac{dI_2}{dt} = U_2 + \kappa_1 U_1^2.
\end{aligned} \tag{2}$$

Here, $f(U) \approx \alpha U + \beta U^3$ is the current through the nonlinear circuit component consisting of semiconductor diodes as a function of the voltage across it, the coefficients $\kappa_{1,2}$ characterize the coupling between the subsystems, and the factor $g \pm ka\cos(\omega_0 t/N)$ represents the conductance of the field-effect transistor controlled by the ac gate voltage $\pm a\cos(\omega_0 t/N)$.

Using the dimensionless variables

$$\begin{aligned}
&\tau = \frac{\omega_0 t}{2\pi}, \quad x = U_1\left(\frac{6\pi\beta}{\omega_0 C_1}\right)^{1/2}, \\
&u = I_1\left(\frac{6\pi\beta}{\omega_0^3 C_1^3}\right)^{1/2}, \\
&y = U_2\left(\frac{6\pi\beta}{\omega_0 C_2}\right)^{1/2}, \quad v = I_2\left(\frac{3\pi\beta}{2\omega_0^3 C_2^3}\right)^{1/2}
\end{aligned} \tag{3}$$

and parameters

$$\begin{aligned}
&A_1 = \frac{2\pi k_1 a}{\omega_0 C_1}, \quad A_2 = \frac{2\pi k_2 a}{\omega_0 C_2}, \\
&h_1 = \frac{2\pi}{\omega_0 C_1}\left(\frac{1}{R_1} - \alpha - g_1\right), \\
&h_2 = \frac{2\pi}{\omega_0 C_2}\left(\frac{1}{R_2} - \alpha - g_2\right), \\
&\varepsilon_1 = \kappa\sqrt{\frac{\omega_0 C_1^2}{6\pi\beta C_2}}, \quad \varepsilon_1 = \kappa_2\sqrt{\frac{C_2}{C_1}},
\end{aligned} \tag{4}$$

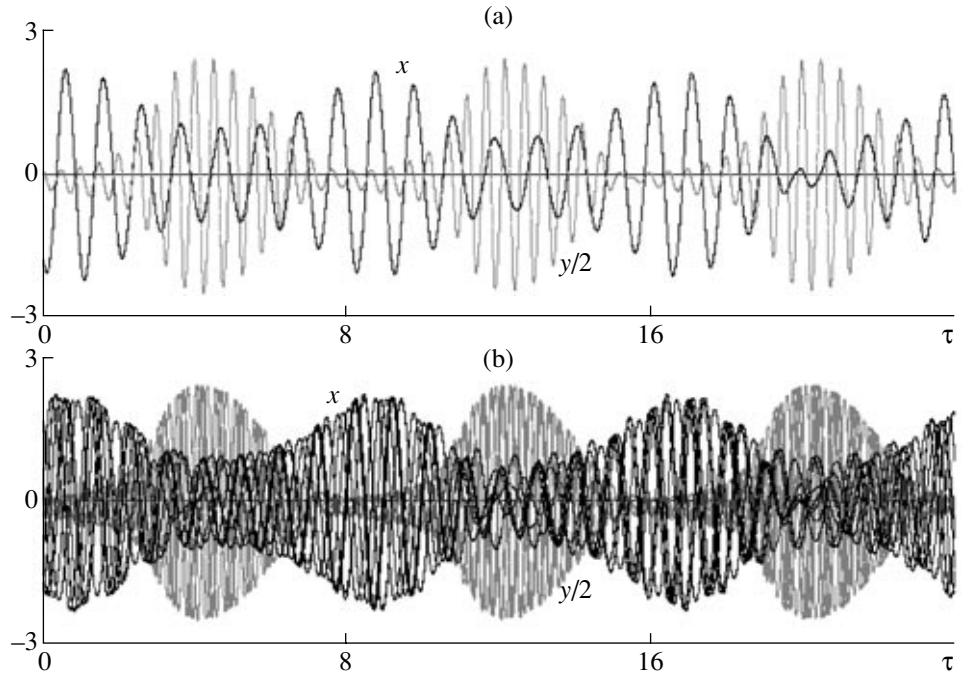

Fig. 3. Time-domain x (solid curves) and y (dotted curves) obtained by computing Eq. (5) for $N = 8$, $A_1 = 1.5$, $A_2 = 6$, $\varepsilon_1 = \varepsilon_2 = 0.1$, and $h_1 = h_2 = 0$: (a) single sample; (b) approximately ten superimposed samples of the same signal realization.

we rewrite the governing equations as

$$\begin{aligned}
&\dot{x} + 2\pi u - \left(h_1 + A_1\cos\frac{2\pi\tau}{N}\right)x + \frac{1}{3}x^3 = 0,\\
&\dot{u} = 2\pi(x + \varepsilon_2 y\cos 2\pi\tau),\\
&\dot{y} + 4\pi v - \left(h_2 - A_2\cos\frac{2\pi\tau}{N}\right)y + \frac{1}{3}y^3 = 0,\\
&\dot{v} = 4\pi(y + \varepsilon_1 x^2).
\end{aligned} \tag{5}$$

Each subsystem is described by two first-order differential equations equivalent to a van der Pol-type equation with time-varying coefficients. The dynamical variables x, u and y, v correspond to oscillators *1* and *2*, respectively. According to the normalization used here, their respective circular frequencies are 2π (which corresponds to the period $\Delta\tau = 1$) and 4π. The factor $h_{1,2} \pm A_{1,2}\cos(2\pi\tau/N)$ is a slowly varying parameter that controls Hopf bifurcation in either subsystem.

4. CHAOTIC ATTRACTOR IN THE MATHEMATICAL MODEL

Figure 3 shows samples of time-dependent x and y obtained by solving Eqs. (5) numerically by the Runge–Kutta method for $N = 8$ and the parameter values $A_1 = 1.5$, $A_2 = 6$, $\varepsilon_1 = \varepsilon_2 = 0.1$, and $h_1 = h_2 = 0$. Figure 3a presents a single sample; Fig. 3b, approximately ten superimposed samples of the same signal on successive time intervals. Figure 3a demonstrates that excitation is alternately transferred between oscillators *1* and *2*. Visual inspection of Fig. 3b suggests that the process is not periodic. A more careful analysis reveals chaotic behavior, which manifests itself in irregular shifts of the maxima and minima of the waveforms $x(t)$ and $y(t)$ generated during successive periods relative to the envelope.

Figure 4a shows the phase portrait of the attractor projected onto the $(x, \dot{x})$ plane. The points plotted in Fig. 4b represent the stroboscopic section of the attractor at successive instants $\tau_n = nN$. The abscissa and ordinate of the plot in Figure 4c are the phases of the signal generated by oscillator *1* at τ_n and τ_{n+1}, respectively, calculated as

$$\varphi = \begin{cases} \arctan\left(-\dfrac{1}{2\pi}\dfrac{\dot{x}}{x}\right), & x > 0,\\ \pi + \arctan\left(-\dfrac{1}{2\pi}\dfrac{\dot{x}}{x}\right), & x < 0. \end{cases} \tag{6}$$

The first-return map in Fig. 4c appears to be topologically equivalent to (1). (A minor discrepancy arises from the somewhat inaccurate qualitative derivation of Eq. (1) and from the definition of the phase; better agreement is achieved for larger values of the period ratio N.)

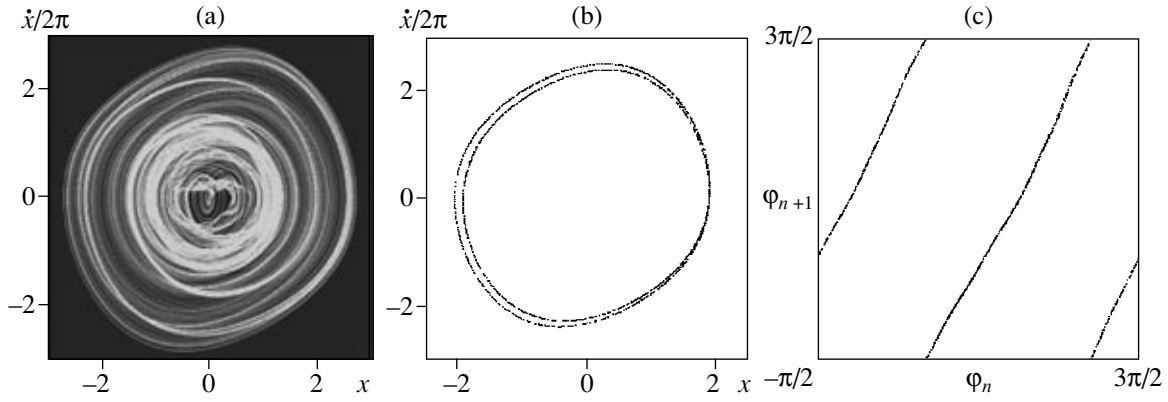

Fig. 4. Attractor corresponding to $N = 8$, $A_1 = 1.5$, $A_2 = 6$, $\varepsilon_1 = \varepsilon_2 = 0.1$, and $h_1 = h_2 = 0$: (a) portrait projected onto the $(x, \dot{x})$ plane of oscillator *1*; (b) stroboscopic section at $\tau_n = nN$; (c) first-return map for the phase of oscillator *1*.

To find the Lyapunov spectrum by Bennetin's algorithm [16, 17], we computed Eqs. (5) simultaneously with the corresponding linearized equations for perturbations,

$$\begin{aligned}
\dot{\tilde{x}} &= -2\pi\tilde{u} - x^2\tilde{x} + \left(h_1 + A_1\cos\frac{2\pi\tau}{N}\right)\tilde{x},\\
\dot{\tilde{u}} &= 2\pi(\tilde{x} + \varepsilon_2\tilde{y}\cos 2\pi\tau),\\
\dot{\tilde{y}} &= -4\pi\tilde{v} - y^2\tilde{y} + \left(h^2 - A_2\cos\frac{2\pi\tau}{N}\right)\tilde{y},\\
\dot{\tilde{v}} &= 4\pi(\tilde{y} + 2\varepsilon_1 x\tilde{x}).
\end{aligned} \tag{7}$$

Performing Gram–Schmidt orthonormalization at each integration step, we averaged the growth rates of the sum of logarithms of norms after orthogonalizing the perturbation vectors, but before normalizing them. It is obvious that the respective Lyapunov exponents for the differential equations and the stroboscopic map, λ_k and Λ_k, satisfy the relation $\lambda_k = N^{-1}\Lambda_k$. For the control parameter values specified above, we obtained $\Lambda_1 \approx 0.69 \approx \ln 2$, $\Lambda_2 \approx -6.64$, $\Lambda_3 \approx -11.12$, and $\Lambda_4 \approx -22.24$. A positive Λ_1 is an indicator of chaos. (Note also that the absence of the zero Lyapunov exponent is natural for maps and nonautonomous continuous-time flows.)

Figure 5 shows Λ_k plotted versus A_1 for $A_2/A_1 = 4$. While the largest Lyapunov exponent Λ_1 has an approximately constant value of about ln2 over a wide interval of parameter variation, others are monotonically varying functions, in agreement with the conjectured hyperbolicity of the observed attractor. The noticeable decrease in Λ_1 toward the left endpoint of the interval signifies a deviation from hyperbolicity.

A hyperbolic chaotic attractor must be structurally stable under changes in the governing equations. Our computations show that this requirement is met. In particular, analogous dynamics are obtained for other integer values of N, including smaller ones. For example, Fig. 6 shows the phase portrait of the attractor corresponding to $N = 4$ projected onto the $(x, \dot{x})$ plane and its stroboscopic section. In this case, $\Lambda_1 \approx 0.69$, $\Lambda_2 \approx -2.40$, $\Lambda_3 \approx -4.24$, and $\Lambda_4 \approx -6.85$. Figure 6b demonstrates the similarity in fine structure between the attractor and the Smale–Williams solenoid depicted in Fig. 1d. Note that fractal fine structure can also be inferred from the first-return map for the phase plotted in Fig. 6c.

The Kaplan–Yorke estimate [3, 7, 8] for the Lyapunov dimension of the stroboscopic section of the attractor is

$$D = 1 + \frac{\Lambda_1}{|\Lambda_2|} \approx 1.29.$$

The Grassberger–Procaccia correlation dimension [3, 7, 8, 18] calculated for the stroboscopic section of

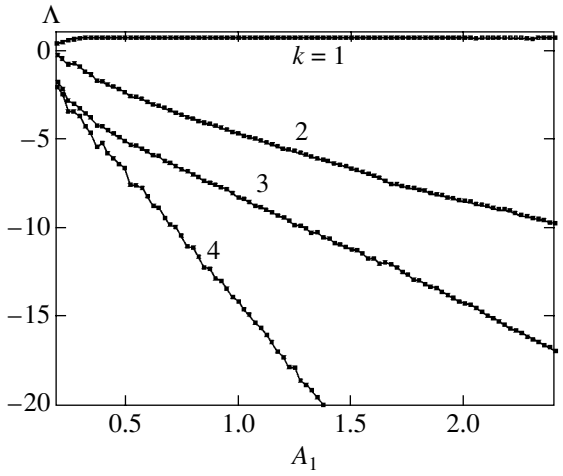

Fig. 5. Computed Lyapunov exponents of the stroboscopic map vs. A_1 for $N = 8$, $A_2 = 4A_1$, $\varepsilon_1 = \varepsilon_2 = 0.1$, and $h_1 = h_2 = 0$. The largest exponent is consistent with the estimated $\Lambda_1 \approx \ln 2$.

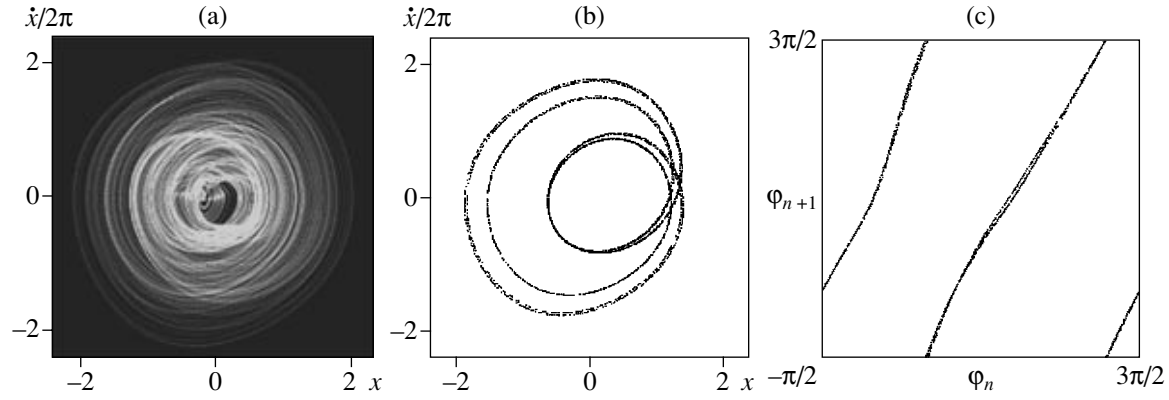

Fig. 6. Attractor corresponding to $N = 4$, $A_1 = 1.5$, $A_2 = 6$, $\varepsilon_1 = \varepsilon_2 = 0.1$, and $h_1 = h_2 = 0$: (a) portrait projected onto the $(x, \dot{x})$ plane of oscillator *1*; (b) stroboscopic section at $\tau_n = nN$; (c) first-return map for the phase of oscillator *1*.

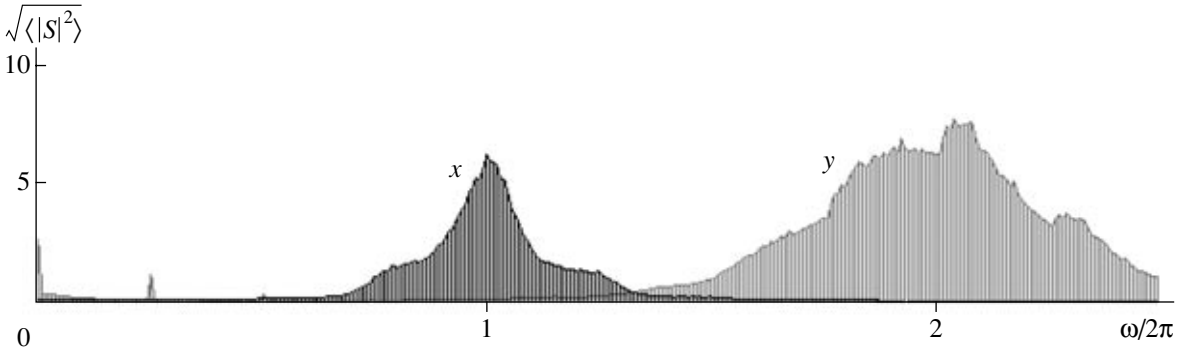

Fig. 7. Spectra of chaotic signals generated in oscillators *1* (x) and *2* (y): $N = 4$, $A_1 = 1.5$, $A_2 = 6$, $\varepsilon_1 = \varepsilon_2 = 0.1$, $h_1 = h_2 = 0$.

the attractor is $D \approx 1.4$, in reasonable agreement with the Lyapunov dimension estimated above. The total dimension of the attractor embedded in the 5D extended phase space of the nonautonomous system is obtained by adding unity: $d = D + 1 \approx 2.4$.

Figure 7 shows the spectra of chaotic signals generated by both oscillators calculated by using a fast Fourier transform algorithm. Note that the spectra of oscillators *1* and *2* in Fig. 7 are continuous and localized around $\omega_0 = 2\pi$ and $2\omega_0 = 4\pi$, respectively. They do not exhibit pronounced multiple peaks characteristic of the spectra of nonhyperbolic attractors. The narrow peaks in the low-frequency tail of the spectrum of oscillator *2* should be attributed to the heterodyning effect of the voltage squarer.

To verify the hyperbolicity of the attractor directly, we applied the numerical procedure suggested in [19, 20] for dynamical systems having a stable direction and an unstable direction at each point of the invariant set. In this procedure, the angle between the directions of small perturbations is calculated at points of a trajectory calculated forward and backward in time. If the results do not contain zero values, then it is concluded that the system is hyperbolic. If the angle distribution demonstrates nonzero probability of zero angle, then the corresponding tangencies between stable and unstable manifolds imply nonhyperbolicity. These tangencies are interpreted as an indicator of a quasi-attractor in a dissipative system.

Since we are dealing with a stroboscopic map in order to compare the results directly with the Smale–Williams solenoid and the only unstable manifold is one-dimensional, while the stable one is three-dimensional, we use the following modified procedure. First, we generate a representative orbit $\{x(\tau), u(\tau), y(\tau), v(\tau)\}$ on the attractor by computing Eqs. (5) over a sufficiently long time interval. Next, we compute Eqs. (7) for perturbations of the orbit forward in time, normalizing the vector $\mathbf{a}(\tau) = \{\tilde{x}(\tau), \tilde{u}(\tau), \tilde{y}(\tau), \tilde{v}(\tau)\}$ at each step to preclude divergence. Then, we compute three replicas of Eqs. (7) backwards in time to find three vectors $\mathbf{b}(\tau)$, $\mathbf{c}(\tau)$, and $\mathbf{d}(\tau)$, performing Gram–Schmidt orthonormalization of the vectors at each integration step to avoid divergence and predominance of one of the vectors.

At each point $\tau_n = nN$ of the stroboscopic section, the vector $\mathbf{a}_n = \mathbf{a}(\tau_n)$ and the span of $\{\mathbf{b}_n, \mathbf{c}_n, \mathbf{d}_n\} = \{\mathbf{b}(\tau_n), \mathbf{c}(\tau_n), \mathbf{d}(\tau_n)\}$ correspond to the unstable direction and the 3D stable manifold, respectively.

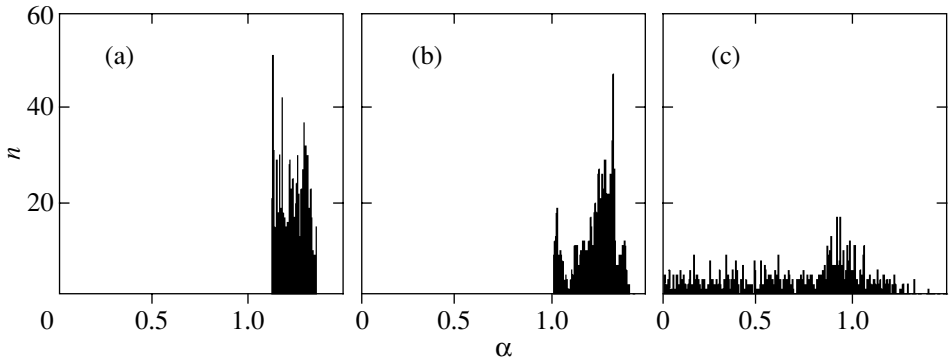

Fig. 8. Histograms of angle α between stable and unstable subspaces for system (5): hyperbolic attractors corresponding to $A_1 = 1.5$, $A_2 = 6$, $h_{1,2} = 0$, $\varepsilon_{1,2} = 0.1$, and $N = 8$ (a) and $N = 4$ (b); (c) nonhyperbolic attractor corresponding to $A_1 = 0.2$, $A_2 = 0.8$, $h_{1,2} = 0$, $\varepsilon_{1,2} = 0.1$, and $N = 8$.

To evaluate the angle α between the unstable and stable manifolds, we determine a vector $\mathbf{v}_n$ transversal to the 3D stable manifold by solving the linear system of equations

$$\mathbf{v}_n \cdot \mathbf{b}_n = 0, \quad \mathbf{v}_n \cdot \mathbf{c}_n = 0, \quad \mathbf{v}_n \cdot \mathbf{d}_n = 0.$$

Then, we calculate the angle $\beta_n \in [0, \pi/2]$ between $\mathbf{v}_n$ and $\mathbf{a}_n$ from

$$\cos\beta = \frac{|\mathbf{v}_n \cdot \mathbf{a}_n|}{|\mathbf{v}_n||\mathbf{a}_n|}$$

and set $\alpha_n = \pi/2 - \beta_n$.

Figure 8 shows the histograms of the computed α_n. The distributions represented by Figs. 8a and 8b correspond to the two sets of control parameter values specified above. Since both distributions are well separated from zero, the hyperbolicity of the attractor can be inferred from the test. For comparison, Fig. 8c shows the histogram plotted for parameter values corresponding to nonhyperbolic dynamics. (In this case, the nonhyperbolicity of the attractor can also be inferred from the behavior of the Lyapunov exponent at the left endpoint of the parameter interval in Fig. 5.)

5. EXPERIMENTAL RESULTS

The circuit design schematized in Fig. 2 was implemented in a laboratory device with $C_1 = 20$ nF, $C_2 = 5$ nF, and ferrite-core coils having equal inductances L_1 and L_2 of approximately 1 H. The free-running frequencies of the oscillators were $f_1 = \omega_0/2\pi = 1090$ Hz and $f_2 = 2f_1 = 2180$ Hz. The negative-resistance amplifier and nonlinear conductance are implemented by using a 140UD26 operational amplifier and KD102 diodes, respectively. A time-varying conductance was introduced by using KP303G field-effect transistors. The nonlinear components responsible for the coupling between the subsystems were based on 525PS2 analog frequency multipliers.

The output voltages U_1 and U_2 were fed into a measuring device (oscilloscope or spectrum analyzer) or into a computer via an ADM12-3 analog-to-digital (A/D) converter with 12-bit resolution and a maximum sampling frequency of 3 MHz. The functions $\dot{U}_1$ and $\dot{U}_2$ were generated by using a standard analog differential amplifier consisting of a 500 pF capacitor and a 62 kΩ resistor combined with a 140UD26 operational amplifier.

Under an appropriate choice of parameters, the experimental system exhibited chaotic oscillations as excitation was alternately transferred between the oscillators by the mechanism discussed above. Figures 9a and 9c show typical examples of the time series obtained by processing chaotic $\dot{U}_1$ and $\dot{U}_2$ waveforms for $N = 8$ and $N = 4$ with the A/D converter operating at a sampling rate of 200 kHz (approximately 200 data points per period corresponding to the free-running frequency ω_0).

Figures 9b and 9d show the first-return maps calculated by substituting into (6) the near-maximum values of $\dot{U}_1(t)$ sampled with the period $T = 2\pi N/\omega_0$ and the derivatives of $\dot{U}_1(t)$ at the same instants produced by the differential amplifier. The topological equivalence of these maps to sawtooth map (1) is essential for inferring the hyperbolicity of the attractor from experimental data.

Figure 10a shows an oscilloscopic trace image of the chaotic attractor corresponding to $N = 4$ (with horizontal and vertical deflections proportional to $\dot{U}_1(t)$ and $U_1(t)$, respectively) photographed with an exposure time of a few seconds to capture a sufficiently large number of the recurrent loops of a trajectory on the attractor. The image obviously resembles that shown in Fig. 6a. Figure 10b shows the stroboscopic section of

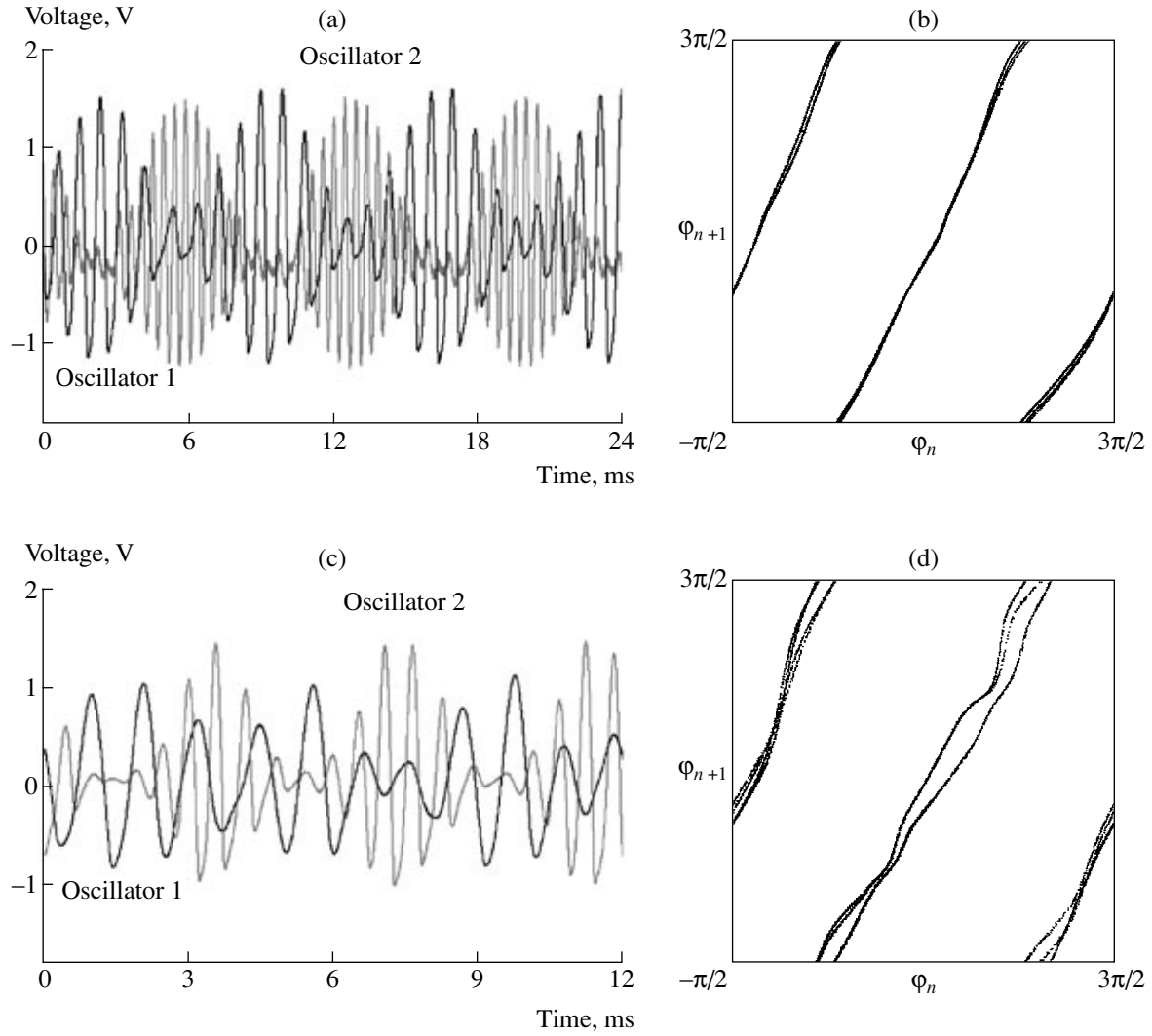

Fig. 9. Examples of time-domain voltage signals generated by oscillators *1* (solid curves) and *2* (dotted curves) operating in the chaotic regime and first-return maps for the phase of oscillator *1*: $N = 8$ (a, b) and 4 (c, d).

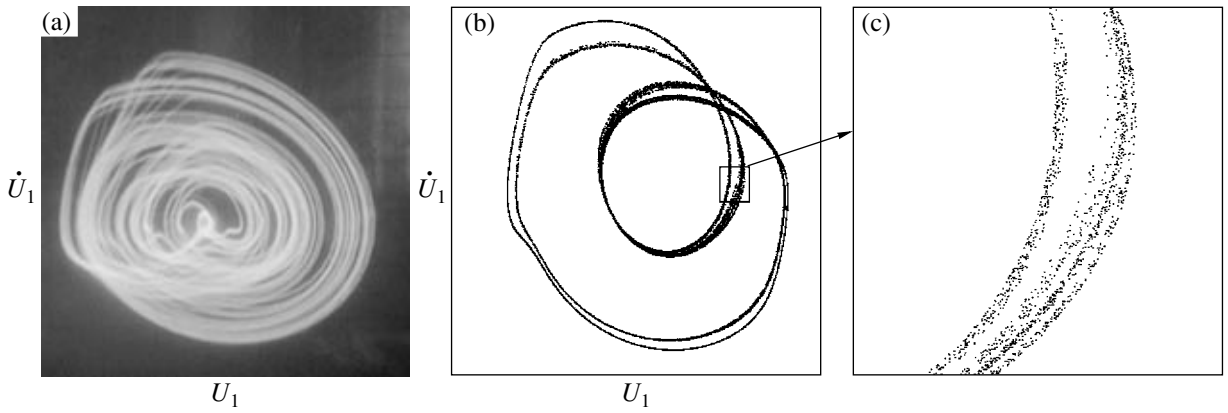

Fig. 10. Portrait of the attractor projected onto the $(U_1, \dot{U}_1)$ plane for $N = 4$: (a) photograph of an oscilloscopic trace image; (b) stroboscopic section with period $T = 2\pi N/\omega_0$ at instants corresponding to near-maximum values of U_1; (c) enlarged fragment demonstrating the fractal fine structure of the attractor.

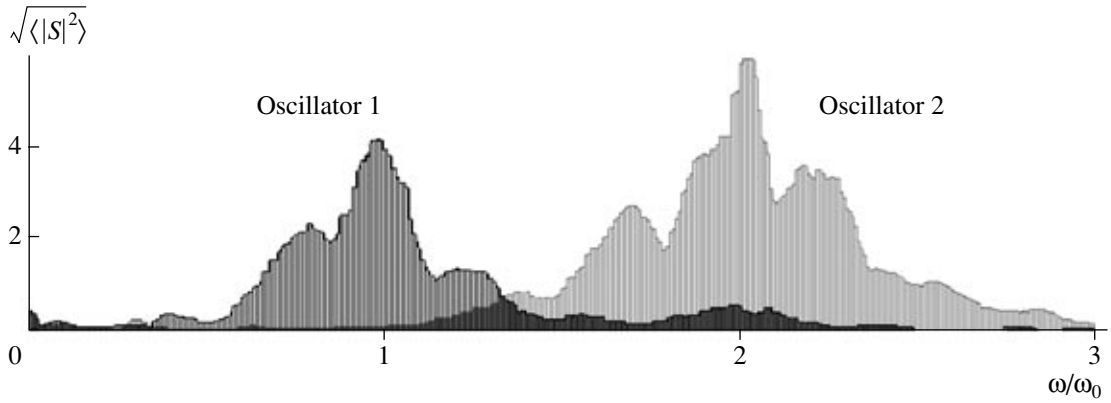

Fig. 11. Spectra of the two oscillators operating in the chaotic regime corresponding to $N = 4$ redrawn from photographs of the spectrum-analyzer display.

the attractor projected onto the $(U_1, \dot{U}_1)$ plane obtained by processing the bivariate time series used to calculate the first-return map in Fig. 9d. It is obviously similar to the analogous portrait of the Smale–Williams solenoid. Figure 10c shows an enlarged fragment demonstrating the fine structure of the attractor.

The Grassberger–Procaccia correlation dimension calculated by processing a time series generated at a sampling rate of 200 kHz is $d \approx 2.3$, in reasonable agreement with that determined from numerical results. The largest Lyapunov exponent of the stroboscopic map [21] evaluated by processing a time series sampled with the period $T = 2\pi N/\omega_0$ is $\Lambda \approx 0.73$, in fair agreement with the estimated value $\Lambda \approx \ln 2$.

Figure 11 combines snapshots of the spectra of waveforms generated by both oscillators operating in the chaotic regime at $N = 4$ in a form suitable for comparison with Fig. 7. Note that the spectra of oscillators *1* and *2* in Fig. 7 are continuous and are localized around $\omega_0 = 2\pi$ and $2\omega_0 = 4\pi$, respectively. They are obviously similar to those obtained by numerical simulation, except for some presumably unimportant features, such as pronounced additional peaks, a secondary maximum in the spectrum of oscillator *1* at the second-harmonic frequency, and the absence of narrow low-frequency peaks in the spectrum of oscillator *2*.

Some numerical results discussed in the preceding section cannot be verified by experiment. For example, it is hardly possible to determine the Lyapunov spectrum or verify hyperbolicity. Nevertheless, in total, the results obtained strongly suggests that the dynamics of the experimental device are similar to those of the Smale–Williams-type attractor in the nonautonomous system analyzed in the theoretical study.

6. CONCLUSIONS

The available characteristics of the dynamics of the physical system examined in this study suggest that it has a strange attractor that can be classified as hyperbolic. A mathematical proof of its hyperbolicity is desirable, but its development is a separate task that lies outside the scope of the present analysis relying on complementary qualitative arguments supported by numerical and experimental results.

We believe that the suggested example of a hyperbolic strange attractor in a physical system is of fundamental importance for further progress in nonlinear dynamics and its applications. For specialists dealing with physical and other systems, this should be a "breakthrough into the realm of hyperbolicity." Using this example as a starting point and taking advantage of the inherent robustness of hyperbolic attractors, one can construct other hyperbolic systems. Indeed, the right-hand sides of governing equations can be modified without losing hyperbolicity, at least if the change is sufficiently small. The availability of physical systems with hyperbolic behavior opens new prospects for applications of the well-developed theory of hyperbolic dynamical systems and provides a basis for comparative studies of hyperbolic and nonhyperbolic chaos in theory and experiment.

ACKNOWLEDGMENTS

We thank B.P. Bezruchko for support of this study, including its experimental part, and V.S. Anishchenko, V.S. Afraimovich, L.A. Bunimovich, R.S. MacKay, L.A. Mel'nikov, A.S. Pikovsky, and M.G. Rosenblum for helpful discussions. This work was supported by the Russian Foundation for Basic Research, project nos. 03-02-16192 and 05-02-16305.

REFERENCES

1. Ya. G. Sinaĭ, in *Nonlinear Waves* (Nauka, Moscow, 1979), p. 192 [in Russian].
2. *Modern Problems of Mathematics. Fundamental Directions. Scientific and Technical Results*, Ed. by R. V. Gamkrelidze (VINITI, Moscow, 1985), Vol. 2 [in Russian].

3. J.-P. Eckmann and D. Ruelle, Rev. Mod. Phys. **57**, 617 (1985).
4. A. B. Katok and B. Hasselblatt, *Introduction to the Modern Theory of Dynamical Systems* (Cambridge Univ. Press, Cambridge, 1995; Factorial, Moscow, 1999).
5. V. Afraimovich and S.-B. Hsu, *Lectures on Chaotic Dynamical Systems* (Am. Math. Soc., Providence, RI, 2003), AMS/IP Studies in Advanced Mathematics, Vol. 28.
6. R. L. Devaney, *An Introduction to Chaotic Dynamical Systems* (Addison-Wesley, New York, 1989).
7. E. Ott, *Chaos in Dynamical Systems* (Cambridge Univ. Press, Cambridge, 1993).
8. S. P. Kuznetsov, *Dynamical Chaos* (Fizmatlit, Moscow, 2001) [in Russian].
9. S. E. Newhouse, Publ. Math. Inst. Hautes Etud. Sci. **50**, 101 (1979); V. S. Afraimovich and L. P. Shil'nikov, in *Nonlinear Dynamics and Turbulence*, Ed. by G. I. Barenblatt, G. Iooss, and D. D. Joseph (Pitman, Boston, 1983), p. 1.
10. V. S. Anishchenko, V. V. Astakhov, T. E. Vadivasova, A. B. Neĭman, G. I. Strelkova, and L. Schimansky-Geier, *Nonlinear Effects of Chaotic and Stochastic Systems* (Inst. Komp'yut. Issled., Moscow, 2003) [in Russian].
11. V. S. Afraĭmovich, V. V. Bykov, and L. P. Shil'nikov, Dokl. Akad. Nauk SSSR **234**, 336 (1977) [Sov. Phys. Dokl. **22**, 253 (1977)].
12. K. Mischaikow and M. Mrozek, Bull. Am. Math. Soc. **32**, 66 (1995); Math. Comput. **67**, 1023 (1998); K. Mischaikow, M. Mrozek, and A. Szymczak, J. Diff. Eqns. **169**, 17 (2001).
13. T. J. Hunt and R. S. MacKay, Nonlinearity **16**, 1499 (2003).
14. T. J. Hunt, PhD Thesis (Univ. of Cambridge, 2000).
15. V. Belykh, I. Belykh, and E. Mosekilde, Int. J. Bifurcation Chaos Appl. Sci. Eng. **15**, 3567 (2005).
16. G. Benettin, L. Galgani, A. Giorgilli, and J. M. Strelcyn, Meccanica **15**, 9 (1980).
17. F. Christiansen and H. H. Rugh, Nonlinearity **10**, 1063 (1997).
18. P. Grassberger and I. Procaccia, Physica D (Amsterdam) **9**, 189 (1983).
19. Y.-C. Lai, C. Grebogi, J. A. Yorke, and I. Kan, Nonlinearity **6**, 779 (1993).
20. V. S. Anishchenko, A. S. Kopeikin, J. Kurths, *et al.*, Phys. Lett. A **270**, 301 (2000).
21. A. Wolf, J. B. Swift, H. L. Swinney, and J. A. Vastano, Physica D (Amsterdam) **16**, 285 (1985).

Translated by A. Betev